Conference on Modelling Fluid Flow (CMFF'22)
The 18th International Conference on Fluid Flow Technologies
Budapest, Hungary, August 30 -September 2, 2022

STEADY AND UNSTEADY PRESSURE LOSS DUE TO A DESIGN OBSTRUCTION VARIATION WITHIN A SMALL-SCALE CHANNEL

Mirza POPOVAC[1], Helmut KÜHNELT[2]

[1] Corresponding Author. Austrian Institute of Technology, Electric Vehicle Technologies, Center for Low-Emission Transport. Giefinggasse 2, 1210 Vienna, Austria. E-mail: mirza.popovac@ait.ac.at
[2] Austrian Institute of Technology, Electric Vehicle Technologies, Center for Low-Emission Transport. Giefinggasse 2, 1210 Vienna, Austria. E-mail: helmut.kuehnelt@ait.ac.at

ABSTRACT

This paper is presenting the results of the numerical study of a flow through a small-scale channel with varying design obstruction. The goal is to analyse the integral flow properties within a channel with obstruction: the steady state pressure loss across the channel with obstruction, and the unsteady force exerted on the obstruction with respect to the obstruction rate of change. The generalization of the impact was examined through the anticipated exponential fitting function. For a comparative evaluation, the characterisation of the pressure loss was sought in a classical engineering form related to the sudden pipe contraction flow (Borda-Carnot expression). However, in order to account for the differences in the respective flow features, the modification of the original expression is put forward and tested.

Keywords: **Borda-Carnot expression, Channel with flap, CFD, OpenFoam, Overset simulations.**

NOMENCLATURE

A	$[m^2]$	incoming flow surface area
A_c	$[m^2]$	contraction surface area
A_s	$[m^2]$	separation surface area
m	[-]	modification exponent
p	$[m^2/s^2]$	kinematic pressure
v_{in}	$[m/s]$	inlet velocity
ΔP	$[Pa]$	total pressure loss
α	$[^o]$	flap angle
μ	$[Pa.s]$	fluid viscosity
ρ	$[kg/m^3]$	fluid density
τ	$[s]$	flap motion time

1. INTRODUCTION

The system of small-scale channels, with the characteristic length of the millimetres order of magnitude, is typically to be found in different cooling applications (e.g. in batteries or as evaporators). If a protruding obstruction appears within these channels, the pressure distribution will be changed in the entire system, which can cause the change of the flow pattern and the cooling characteristics overall. For example, by changing the pressure difference between the incoming and the outflowing evaporator header, its active area (and hence the temperature distribution within the entire evaporator) can change significantly. In order to investigate the effect of the additional pressure loss within a small-scale channel due to an obstruction, a numerical analysis was performed on a simple plain channel geometry with a flap motion representing the protruding obstruction. Being a niche application, to the best of authors' knowledge, there are no publicly available results on the related topic. However, this problem can be viewed as a flow around the flap valve, the application of which can be found in a number of large-scale engineering problems, ranging from the flows in the HVAC systems [1] to the nuclear vessel flows [2].

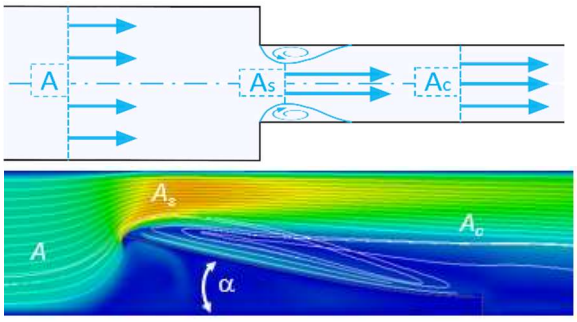

Figure 1. Sketch of a sudden pipe contraction flow (top) and flow over a flap within a channel (bottom)

Depicted in Figure 1 is a resemblance between the flow through a sudden pipe contraction and the flap-channel case: the incoming flow (with the cross-section surface area A) features the reduction of the flow cross-section, and passing the edge of the

contraction the flow separates and causes further reduction of the flow cross-section (vena contracta, A_s), before recovering subsequently to the final contraction flow conditions (having the cross-section surface area A_c). The similarity can be found (in particular with the symmetrical part of the pipe contraction) by looking at the small-scale channel, with a flap under given angle α for modeling the obstruction: at the flap leading edge the flow is being pushed upwards, flowing over the flap surface a separation zone is created, and further downstream the flow recovers its contracted state (eventually developing fully if the channel length permits).

For the sudden pipe contraction flow the empirical correlation of Borda-Carnot is based on a well-established engineering practice to corelate the total pressure loss ΔP to the kinetic energy of the flow defined by the incoming flow velocity v_{in} [3]:

$$\frac{\Delta P}{\rho} = \frac{v_{in}^2}{2}\xi_{BC}$$
$$\xi_{BC} = \left(1-\frac{1}{\sigma}\right)^2\left(\frac{A}{A_c}\right)^2 \qquad (1)$$
$$\sigma = \frac{A_s}{A_c} = (n-1) + n\left(\frac{A_c}{A}\right)^q$$

where ρ is the fluid density, and ξ_{BC} is the Borda-Carnot loss coefficient expressed in terms of the geometrical quantities which are characterizing the sudden pipe contraction, i.e. the incoming flow and the contracted surface areas A and A_c. respectively. In the literature one can find different methods for calculating the smallest surface area at the location of the flow separation A_s [4]. In this work, following the measurements of Weisbach [5], it is expressed in terms of the contraction ratio σ, which is for a sharp-edged contraction approximated as a weighted average between the relative incoming (A/A) and contracted flow area (A_c/A) with $n=0.37$ and $q=3$.

For a flap-channel flow the contracted surface area is related to the flap angle α, following $1-\sin\alpha$ if the flap is fixed to the bottom wall. In the flap-channel case, however, the contraction recovery is not directly limited by the downstream geometry. Therefore, in the original Borda-Carnot framework, Eq.(1), the modification is put forward:

$$\frac{A_c}{A} = (1-\sin\alpha)^m \qquad (2)$$

where the contraction ratio exponent m is introduced to capture the effect of the flow contraction which is not geometrically confined.

Based on the observation that the flow after flap will spread further downstream, given that the expression between the brackets in Eq.(2) is less than unity, also m needs to be less than unity to account for the spreading of the contraction zone. The value adopted for the modification exponent in Eq.(2) is $m=0.5$, although it is expected to feature some dependency on the channel mass flow rate. In this work, however, the focus is only on the plausibility testing, while further fine tuning is yet to be done.

2. SIMULATION SETUP

Resembling a flap valve placed within the straight section of the duct connecting two large reservoirs, the adopted geometry is sketched in Figure 2. The domain consists of a plane channel of *6 mm* height and *65 mm* length. Located at the channel's half-length is *0.1 mm* thick flap, which can rotate around its lower edge shifted *0.15 mm* from the bottom wall. Next to the rotation axis is *0.1 mm* thick block, with *0.15 mm* clearance to the flap (allowing for the "leakage" around the flap valve shaft). The block is reducing the flow under the flap, thus supporting the flow development over the leading edge of the flap. The flow effects in the spanwise direction are neglected.

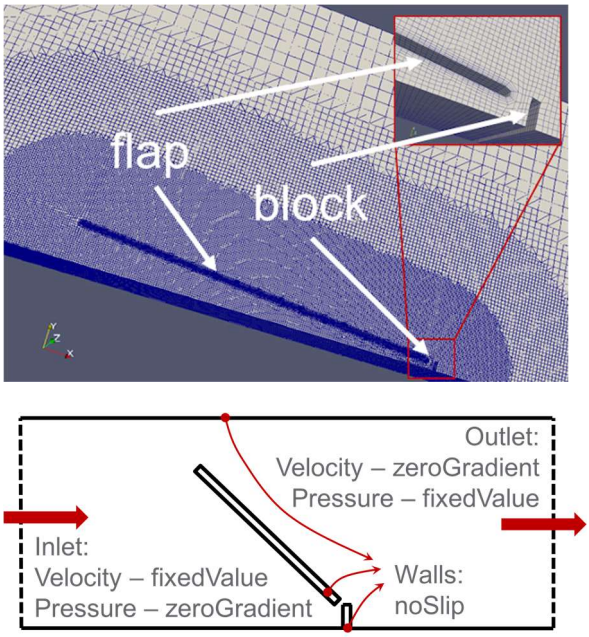

Figure 2. Numerical mesh (top) and boundary conditions (bottom) for the flap-channel case.

The simulations have been performed using open-source CFD library suite *OpenFoam* [6]. The hex-dominant mesh shown in Figure 2 (generated with *snappyHexMesh*) is featuring different levels of cell refinement based on the distance from the flap and boundary layer cells around the flap. This is ensuring sufficient near-wall mesh resolution: y^+ below 1 on the flap, and on other walls below 10. As for the boundary conditions, constant velocity v_{in} was imposed at the inlet, and at the outlet the constant (zero) pressure was specified. All walls are treated as no slip boundaries, and in the spanwise direction symmetry was imposed. The constant fluid

properties of water have been assumed: density $\rho=998.2\ kg/m^3$, and $\mu=1.01\ mPa.s$ for the dynamic viscosity. The steady state simulations have been performed using incompressible isothermal Newtonian fluid flow solver based on SIMPLE pressure-velocity coupling (*simpleFoam*). Since the flow properties are taken constant, instead of the total pressure P the kinematic pressure $p=P/\rho$ was used as the flow variable in solving the momentum and continuity equations (the same way as the kinematic viscosity $\nu=\mu/\rho$ was used instead of μ). This approach was extended for the unsteady simulations, capturing the flap motion using the overset method for overlapping meshes (*overPimpleDyMFoam*). In order to ensure the convergence of the simulation, the time stepping was controlled through the $CFL=1$ stability criterion.

3. FLOW CHARACTERISTICS

The distributions of the velocity magnitude and pressure are shown in Figure 3 for the flow case with the flap angle 10°, representing low flap angles. The obtained results indicate that the low flap angle cases feature the flow effects similar to the sudden pipe contraction flow. Namely, the incoming flow separates at the leading edge of the flap, and after the recirculation bubble on the flap surface, it recovers to its contraction state downstream. This is also mirrored in the pressure distribution, showing a transition from the high-pressure region upstream, over the under-pressure in the separation zone on the flap, finally to the imposed zero value at the outlet.

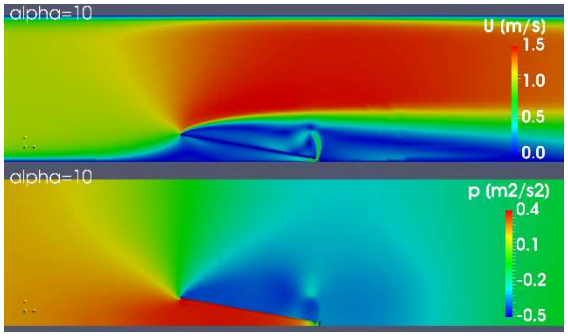

Figure 3. The velocity magnitude (top) and the kinematic pressure (bottom) for the flap-channel case with low flap angle (α=10°).

Completely different is the flow pattern obtained for the high flap angles, as shown in Figure 4 for the flow case with 80° flap angle. Given that a constant velocity was imposed at the inlet, the mass flow rate through the domain is also constant, and therefore most of the flow is squeezed through the gap between the flap edge and at top wall (since the small gap at the bottom wall allows for relatively small mass flow from below). Being ejected from the flap leading edge, the high velocity fluid creates a massive recirculation zone behind the flap leaving the flow pattern without "classical" contraction region (assumed for the Borda-Carnot expression). This behavior is reflected in the pressure distribution, where the high pressure up-stream is sharply divided from the low pressure behind the flap.

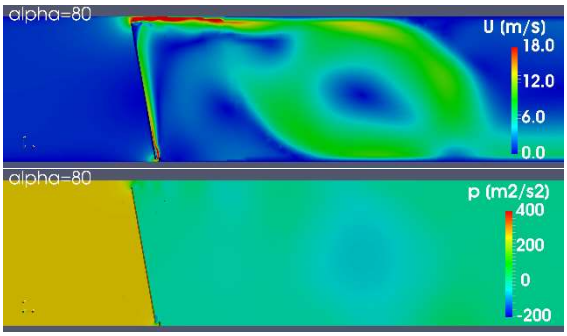

Figure 4. The velocity magnitude (top) and the kinematic pressure (bottom) for the flap-channel case with high flap angle (α=80°).

With the described numerical setup the flap-channel pressure loss characteristics is obtained from the series of simulations, aiming to generalize it through the anticipated exponential fitting function. Regarding the casting of the obtained characteristics into the modified Borda-Carnot pressure loss, the differences in the flow patterns between the low and high flap angle cases are setting low the expectations for this simplified engineering approach.

3.1. Steady state pressure loss

The assessment of the steady state pressure characteristics for a range of inlet velocities was performed through the series of subsequent simulations with different flap angle α. In Figure 5 the kinematic pressure at the flap-channel inlet (corresponding to the pressure loss across the flap-channel, since the outlet pressure is set to zero) is plotted over all investigated flap angles (dots). For the obtained results the anticipated exponential function was fitted (dashed lines), and the coefficient of determination R^2 shows good agreement over the investigated flap angle range for all calculated inlet velocities. As for the modified Borda-Carnot approximation (full lines), there is a good agreement up to approximately 45° flap angle (half of the investigated flap angle range), after which it starts to depart strongly. Looking closer at the agreement range (shown enlarged in Figure 5), one can see that the modified Borda-Carnot expression fits the stimulation predictions within 10% accuracy. Important to note, though, is the agreement departure of the modified Borda-Carnot predictions for different inlet velocity cases. This is an indication that instead of the assumption of a constant value of the modification exponent m, more appropriate seem to be its dependency on the mass flow rate through the channel.

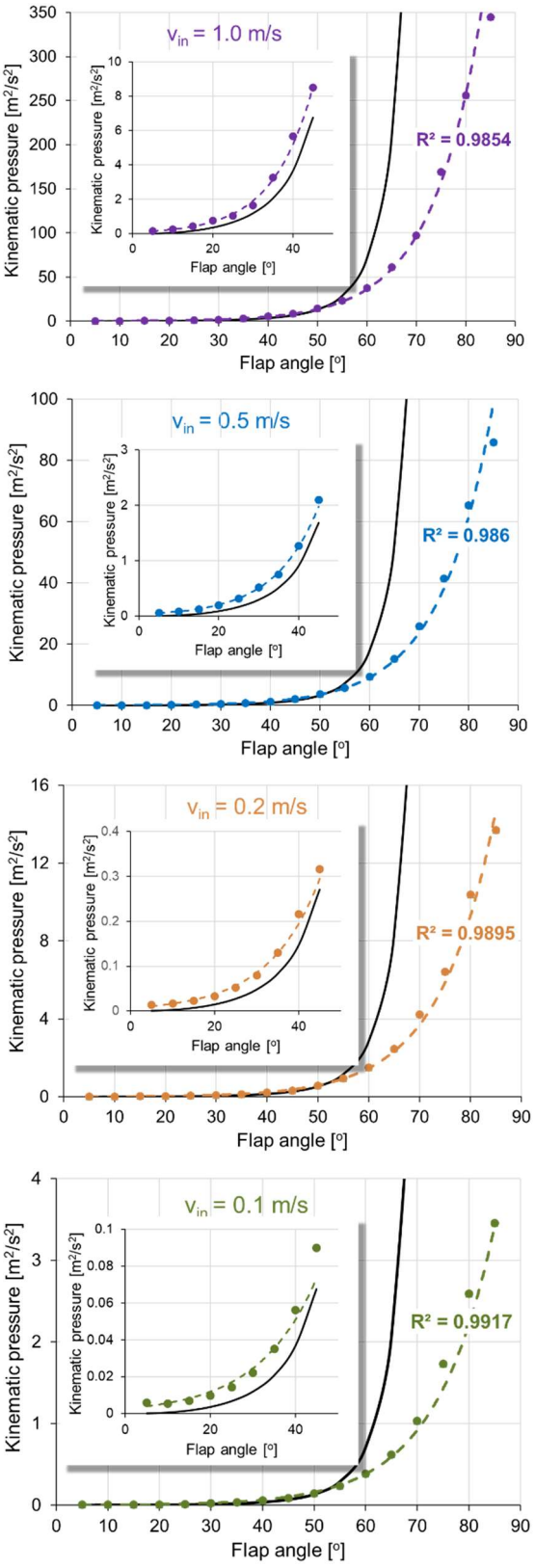

Figure 5. Steady state kinematic pressure (corresponding to the pressure loss across the flap-channel) for different inlet velocities (top to bottom: *v_{in}=1.0, 0.5, 0.2, 0.1*, coloured violet, blue, orange and green respectively): simulations – dots, exponential fit – dashed line, modified Borda-Carnot – full line.

Having adopted the anticipated exponential fit for the obtained curves, the generalization of the calculated pressure loss values ΔP_{calc} is accomplished through the normalization with the squared inlet velocity v_{in}. This is equivalent to the definition of the pressure loss coefficient ξ, which is also sought in the exponential form:

$$\xi = \frac{\Delta P_{calc}/\rho}{v_{in}^2/2} = C_1 e^{\alpha C_2} \qquad (3)$$

where C_1 and C_2 are respectively the base coefficient and the exponent in the anticipated exponential function.

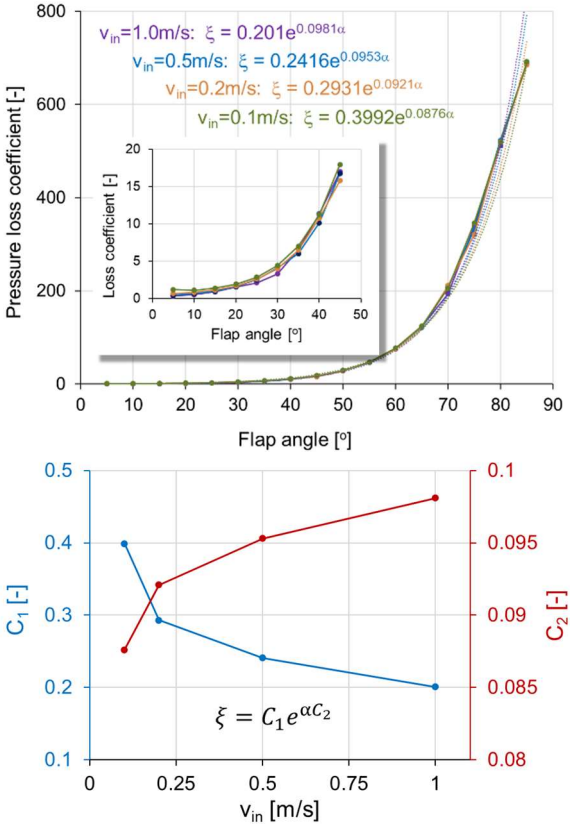

Figure 6. Steady state pressure loss coefficient in the flap-channel for different inlet velocities (top) and the coefficients of the pressure loss exponential fit depending on the inlet velocity (bottom).

As shown in Figure 6 (top), these normalized curves are tending to collapse to a single one for the entire calculated flap angle range. A closer look reveals particularly good agreement for the pressure loss coefficient at the smaller flap angles, while for higher flap angles the deviation is more pronounced. However, from the plot of coefficients as a function of the inlet velocity v_{in} (Figure 6, bottom) one can note that the base coefficient C_1 (blue) has a large spreading over different inlet velocities. The relative standard deviation of C_1 over v_{in} amounting to 30% can be seen as the quantification of the above-

mentioned dependency of m on the inlet velocity. For the exponent C_2 (red), however, this spreading is less pronounced (relative standard deviation less than 5%). As a result, it can be assumed that the exponent of the fitting function for ξ is generally valid for the investigated case.

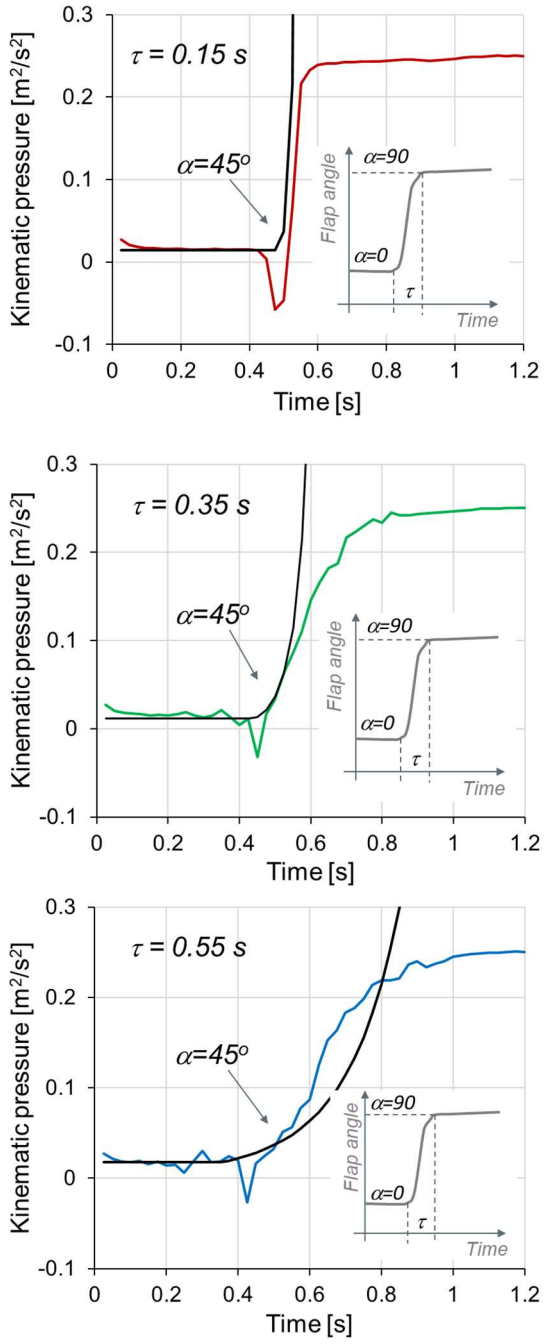

Figure 7. Unsteady kinematic pressure (corresponding to the pressure loss across the flap-channel) with fixed inlet velocity v_{in}=1.0m/s for different flap angular change rate (top to bottom: τ=0.15s, 0.35s, 0.55s, coloured red, green and blue respectively) compared to the modified Borda-Carnot expression (black).

3.2. Unsteady pressure loss

In order to analyze the pressure loss behavior in the flap-channel under unsteady flow conditions, as well as to test the applicability of the proposed Borda-Carnot modification there, the flap-channel simulations have been repeated with the same numerical setup (constant inlet velocity v_{in}=1.0m/s), only for the flap the angular motion was imposed through the predefined sigmoid function:

$$\alpha(t) = \alpha_{end}\frac{1 + erf\left(\frac{t - t_0}{0.25\tau}\right)}{2} \qquad (4)$$

where α_{end}=90° is the end position of the flap, and the error function varies between -1 and 1 within the time interval τ (characteristic increase time) around the specified time instant t_0 (here selected t_0=0.5s).

Since the mass flow rate remains constant in this case (set with v_{in}=1.0m/s), the overall pressure loss increases with the imposed flap motion. Its time evolution is shown in Figure 7 for different characteristic increase times (red, green and blue for τ = 0.15s, 0.35s and 0.55s respectively), and the corresponding forces acting on the flap, normalized with the maximum force occurring at α_{end}=90°, are shown in Figure 8. The comparison with the proposed Borda-Carnot modification (Figure 7, black) indicates qualitatively the same output as in the steady state case: the modified Borda-Carnot predictions follow the magnitude of the pressure loss increase only up to a certain limit (about 45° flap angle), after which they fail completely.

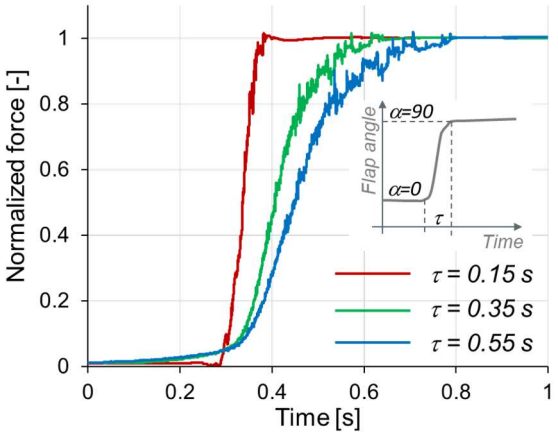

Figure 8. Unsteady normalized force acting on the flap surface in the flap-channel with fixed inlet velocity v_{in}=1.0m/s for different flap increase times (τ=0.15s, 0.35s, 0.55s, coloured red, green and blue respectively).

An interesting feature in these unsteady numerical simulations is observed as the under-pressure peak in the pressure loss temporal evolution at the beginning of the flap angular motion (around t=0.4s). As the flap is forced into its motion, a cavitating under-pressure field is established, before

the pressure starts to rise due to the increased flow resistance from the flap. It is the flap angular change rate (through Eq.(4) determined by τ) that characterizes this under-pressure peak, together with the relaxation time needed for reaching the final pressure loss.

4. CONCLUSIONS

This work presented the analysis of the pressure loss within a small-scale channel with protruding obstruction, here modelled through the motion of a flap within the channel. Furthermore, an attempt was made to generalize the pressure loss characterization through the exponential function. Finally, the applicability of the Borda-Carnot empirical expression for the pressure loss within pipes with sudden contraction, was tested for this flap-channel flow case.

It has been observed that the exponential function describes well the variation of the static flap-channel pressure loss for different channel mass flow rates, in particular for the lower flap angles. However, while in the exponential fit it can be assumed that the exponent features universal validity for the investigated case, the base coefficient has a large spreading over different inlet velocities. In addition to the steady-state characteristics, for the unsteady flap-channel flow one can identify the under-pressure peak as a consequence of the imposed flap angular motion. Its intensity depends on the flap angular change rate, influencing thus the pressure relaxation time.

In the view of similarity between the flap-channel case and the flow through the sudden pipe contraction, the modification of the original Borda-Carnot expression was introduced to account for the recovery of the contracted flow which is not directly limited by the geometry. The obtained results suggest a dependency of the modification exponent m on the channel mass flow rate. Nevertheless, as a proof of concept, with a constant value for m, acceptable pressure loss predictions are obtained for low flap angles (corresponding to small protruding obstructions), although. For high flap angles (big protruding obstructions) the characterization of the flow contraction loses its validity, as the massive recirculation zone is created behind the flap, and the pressure loss predictions fail completely.

ACKNOWLEDGEMENTS

The presented work has been financially supported through the EU Programme Horizon 2020, Project SELFIE (Grant Agreement number: 824290).

REFERENCES

[1] Lukács E. and Vad J. (2021), "Flow topology and loss analysis of a square-to-square sudden expansion relevant to HVAC systems: A case study", *Journal of Building Engineering*, Vol. 41, https://doi.org/10.1016/j.jobe.2021.102802.

[2] Belliard M., (2018), "Numerical modeling of an in-vessel flow limiter using an immersed boundary approach", *Nuclear Engineering and Design*, Vol. 330, pp. 437-449, https://doi.org/10.1016/j.nucengdes.2018.01.027.

[3] Batchelor, G. K. (1967), *An Introduction to Fluid Dynamics*, Cambridge University Press, ISBN 978-0-521-66396-0.

[4] Dayev Zh. A. and Kairakbaev A. K. (2019), "Modeling of coefficient of contraction of differential pressure flowmeters", *Flow Measurement and Instrumentation*, Vol. 66, pp. 128-131, https://doi.org/10.1016/j.flowmeasinst.2019.02.009.

[5] Oertel H., Prandtl L., Böhle M. and Mayes K. (2004), *Prandtl's Essentials of Fluid Mechanics*, Springer, ISBN 978-0-387-40437-0.

[6] OpenCFD (2019), *OpenFOAM: The Open Source CFD Toolbox - User Guide v1906*, OpenCFD Limited. Reading UK.